International Journal of Thermophysics, Vol. 7, No. 5, 1986

Hydrogen Component Fugacities in Binary Mixtures with Methane and Propane

T. J. Bruno,[1] G. L. Hume,[1] and J. F. Ely[1]

Received October 9, 1985

The fugacity coefficients of hydrogen in binary mixtures with methane and propane were measured using a physical equilibrium technique. This technique involves the use of an experimental chamber which is divided into two regions by a semipermeable membrane. Hydrogen can penetrate and pass through the membrane, while the other component (in this case, methane or propane) cannot. At equilibrium, pure hydrogen will permeate into one "compartment" of the chamber, while the binary mixture occupies the other compartment. Thus, the pressure of pure hydrogen on one side approaches the partial pressure of hydrogen in the mixture on the other side of the membrane. This allows a direct measurement of the hydrogen component fugacity at a given mixture mole fraction. In this study, results are reported for measurements made on the hydrogen + propane binary at 80°C (353 K) and 130°C (403 K) and the hydrogen + methane binary at 80°C (353 K). All measurements were performed with a total mixture pressure of 3.45 MPa. The experimental results are compared with predictions from the Redlich–Kwong, Peng–Robinson, and extended corresponding-states models.

KEY WORDS: fugacity coefficients; fugacity measurements; gas chromatograph; gas mixtures; hydrogen; methane; propane.

1. INTRODUCTION

Fugacity is an important function in both experimental thermodynamics and engineering science. The importance of this quantity stems from the theoretical basis of fugacity [1–3] and the general usefulness of fugacity in describing chemical systems with appreciable nonideality [4–6]. The general criteria for phase equilibrium of any system are greatly simplified by explicit consideration of fugacity [7]. Thus, for a system to be at

[1] Thermophysics Division, National Bureau of Standards, Boulder, Colorado 80303, U.S.A.

0195-928X/86/0900-1033$05.00/0

equilibrium, the requirements of phase equality of temperature, pressure, and component fugacity must be met. In a system involving chemical reactions, fugacities appear in the equilibrium constants describing the multicomponent system. Departures from equilibrium can be described in terms of fugacity gradients [8]. Since fugacity is a measure of the nonideality of a system, measurements of fugacity and fugacity coefficients are of value in research on equations of state, especially work involving mixtures.

The physical equilibrium method of measuring fugacity is a direct technique which is especially useful in the study of gaseous mixtures containing hydrogen. The principle of the method is quite simple and has been discussed in detail elsewhere [9]. An experimental chamber (such as a pressure vessel) is divided into two regions by a membrane permeable only to hydrogen. The membrane is invariably in the form of a metal tube or thimble [10, 11]. If one side of the membrane (in the pressure vessel) is charged with a gaseous mixture (of which hydrogen is a component) and the other side is initially evacuated, an equilibrium will eventually be established between the two sides of the membrane. The approach to equilibrium is driven by the need to equalize the chemical potential of hydrogen on either side of the membrane. At equilibrium, the pressure of pure hydrogen on one side of the membrane will equal (in the limit of the ideal gas) the partial pressure of hydrogen in the mixture on the other side of the membrane. At this point, the fugacity of hydrogen on both sides of the membrane must be equal. Using appropriate instrumentation, the hydrogen partial pressure, P_{H_2}, and the mixture total pressure, P_m, can be measured at a given temperature T and a given mixture hydrogen mole fraction x_{H_2}. From these measurements and a knowledge of the equation of state of pure hydrogen, the component fugacity of hydrogen can be calculated.

Rather than working with the fugacity, it is usually more convenient to deal with a dimensionless quantity called the fugacity coefficient, ϕ_i, defined by

$$\phi_i = f_i/(x_i P_i) \tag{1}$$

For a pure component (in the present case, i is hydrogen) the fugacity coefficient can be determined using the virial equation truncated after the third virial coefficient:

$$\ln \phi_{H_2} = \frac{B}{R}\left(\frac{P_{H_2}}{T}\right) + \frac{C - B^2}{2R^2}\left(\frac{P_{H_2}^2}{T^2}\right) \tag{2}$$

where B and C are the second and third virial coefficients, and R is the gas constant. The above quantity is for pure hydrogen only, at pressure P_{H_2}.

Clearly, P_{H_2} is necessarily lower than P_m, due to the presence of the second component in the binary. To determine the fugacity coefficient of hydrogen in the mixture, we apply the defining equation for the mixture fugacity coefficient:

$$\phi^m_{H_2} = \hat{f}_{H_2}/x_{H_2}P_m \tag{3}$$

to obtain

$$\hat{f}_{H_2} = f_{H_2} = x_{H_2}P_m\phi_{H_2}$$

where ϕ_{H_2} is given by Eq. (2).

2. EXPERIMENTAL

The apparatus used in this study has been described elsewhere in detail [12–14], so only a brief general description is provided here. The apparatus is depicted schematically in Fig. 1. The heart of the apparatus is a large (2050-ml internal volume) thick-walled pressure vessel, designed in accordance with ASME guidelines [15] specifically for this application. The vessel, which uses a bolted gasket closure, is constructed of 316-L (AISI designation) stainless steel. The vessel, with its closure, is capable of containing a pressure of 50 MPa at 350°C (623 K). The vessel lid accommodates necessary feedthroughs and a propeller-type mixer driven by a commercial magnetic linkage.

The semipermeable membrane, required for the partial-pressure measurements, was made from 396-cm-long sections of palladium/silver (75/25) alloy tubing. The tubing has an outside diameter of 0.160 cm, with a wall thickness of 0.008 cm. The membrane manifold consists of three formed coils of this tubing, brazed to a length of stainless-steel tubing. This piece of stainless-steel tubing provides for the measurement of the internal pressure of the membrane using a feedthrough in the lid of the pressure vessel. A detailed discussion of the complexities of construction of this manifold is provided elsewhere [12]. A second feedthrough in the vessel lid allows access to the main pressure vessel volume (outside the membrane) to allow measurement of the total mixture pressure.

Measurements of the pressure of the pure hydrogen (from inside the membrane manifold) and the mixture (outside the membrane) were made using a commercial dead weight pressure balance. The balance has an accuracy of 0.015% and a range of between 0.04 and 82.7 MPa. The pressure of the test fluid (either hydrogen or mixture) is referenced to an innert gas line via a diaphragm-type differential pressure transducer. The inert gas communicates its pressure to another differential pressure trans-

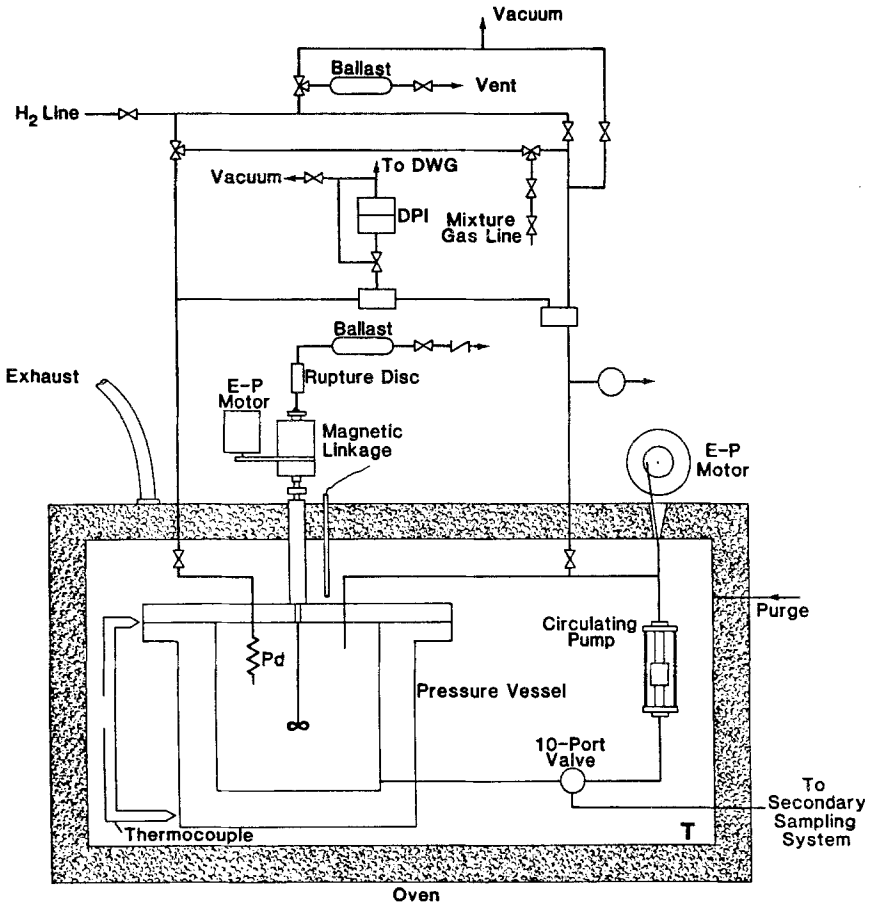

Fig. 1. Schematic diagram of physical equilibrium fugacity apparatus.

ducer which is referenced to oil pressure. The oil pressure is generated by weights on a piston table. When both differential pressure transducers are at null condition, one can obtain the pressure of the test fluid by summing the weights pressurizing the piston. Corrections are made for local gravity (979,601.148 milligals at Boulder station B), atmospheric pressure, temperature effect on piston area, elastic distortion of the cylinder, and oil head pressure. Corrections for fluid expansion into valve and transfer line volumes are also required. In actual practice, the differential pressure transducers are first brought to null with equal opposing pressures, to allow the setting of a zero reference point. Hysteresis effects in the transducer are

minimized by "rocking" the diaphragm up and down several times before taking a measurement. The effect of temperature on the pressure transfer lines (between differential pressure transducers) is a small source of systematic error, so care was taken to maintain a uniform room temperature.

A commercially available *vigorously mixed oven* was modified to provide a thermostat. The major modifications included the installation of baffles (to promote more uniform mixing of the temperature transmitting fluid), the installation of large aluminium thermal masses (to reduce temperature gradients), and the fabrication of a thermally insulated cover plate (from which the pressure vessel and other high-temperature components are suspended inside the oven).

The oven is heated by 6.5-kW resistive elements controlled by a proportional SCR circuit, allowing temperature control of the apparatus components to ± 0.05 K. The controller is also equipped with a high-temperature limiting cutoff for safety. For additional safety, the temperature transmitting fluid of the oven is maintained at a slight negative pressure, and a low flow rate of nitrogen is continually passed through the hot zone and is exhausted into a fume hood.

Temperature gradients among key components inside the oven are monitored using oposed pairs of J-type (iron–constantan) thermocouples [16]. The observed gradients are then minimized using very low-power "shimming" heaters located near or in major components.

Temperature measurements are made using a commercial quartz crystal oscillator thermoprobe. The quartz probe is located in a thermowell in the pressure vessel. The immersion error of the probe in this configuration was calculated to be of the order of ± 0.003 K. A single point calibration is performed on a regular basis, using either the triple point or the freezing point of water. This single point measurement is for scaling only; the frequency versus temperature table for the quartz probe is stored on a ROM and is accessed automatically. The probe has an absolute accuracy of ± 0.03 K in the present region of interest. Errors due to long-term instability amount to less than ± 0.008 K. Errors due to hysteresis are of a negligible level, since the measurements are made isothermally. Thus, thermometry precision of the order of $\pm 0.05\%$ (coefficient of variation) is easily obtainable.

Since an accurate measurement of the hydrogen mole fraction, x_{H_2}, is required to deduce fugacity coefficients, a custom-designed developmental gas chromatograph and sampling system were constructed. The chromatograph was constructed to provide precise column temperature and carrier flow rate control. The sampling system consists of two parts. The first part, shown in place in Fig. 1, allows the gas mixture to be cir-

culated through the sample loop of a commercial 10-port sampling valve. Sample circulation is accomplished using a check valve pump, which minimizes concentration gradients that often plague expansions of gas mixtures from higher pressures. The sampling valve shown in Fig. 1 is actuated remotely using pressurized helium, which provides very fast switching. This valve transfers an aliquot of mixture to a second sampling system which provides for temperature and pressure control of the sample and ultimate injection into the chromatograph. A detailed description of this unit is provided elsewhere [13].

The column is thermostated in a vigorously stirred oil bath which is maintained to within ± 0.02 K. All analyses are done isothermally to minimize carrier flow-rate disruptions. Column pressure is controlled using a fine-adjustment pressure regulator (a commercially available unit used for pressure gauge calibration) followed by a fine metering valve. The chromatograph is very similar to units used for thermodynamic measurements [17]. Mass flow controllers are not used since the column temperature is not programmed. The carrier gas flow rate, measured at the detector exit, is maintained at 40.00 ± 0.05 ml/min. Since both hydrogen and the mixture gas required detection and quantitation, argon was chosen as the carrier gas [18].

The separation of mixtures of hydrogen–methane and hydrogen–propane is experimentally trivial and is described later. A microcell thermal conductivity detector (TCD) at the column exit, connected to a commercial electronic integrator, provided detection and quantitation. Peak area counts as logged by the integrator are corrected for atmospheric pressure (equivalent to sample loop pressure, since injections were done at ambient pressure) and detector aging. The pressure correction is required since the loop pressure affects the quantity of fluid injected, and dividing by the atmospheric pressure normalizes the response. The correction for detector aging is needed since the gold-sheathed tungsten filaments of the TCD run hotter in an argon carrier stream then in the more common carrier gases such as helium and hydrogen. Thus, the filaments undergo accelerated oxidation due to trace amounts of oxygen that are not trapped. This correction is applied by periodically injecting a standard mixture to track signal loss. The corrected peak areas are then converted to mole fractions using either a calibration equation or the standard bracketing technique [19]. After leaving the detector exit, sample and carrier are expelled through a transfer line to a dedicated outside blower, to provide operator safety.

The separation of the hydrogen/methane binary mixture was easily done using a packed column (1.5 m long, 0.32-cm o.d.) of 150- to 200-mesh 5-Å molecular sieve. The column was maintained at 60°C (333 K), since

methane was found to adsorb on the zeolite surface at lower temperatures. Calibration was done using the external standard method [20, 21] using 10 standard mixtures which were prepared gravimetrically.

The separation of the hydrogen/propane binary mixtures was performed using a packed column (1.5 m long, 0.32-cm o.d.) of Porapak-Q.[2] The column was maintained at 80°C (353 K), since the porous polymer packing was observed to entrain hydrogen at lower temperatures. It should be noted that elevated temperatures cause the polymer beads to swell, resulting in an increase in the retention time of hydrogen and a decrease in that of propane. Thus, the temperature at which the two peaks merge is lowered by these additive effects.

In the case of hydrogen/propane, calibration was done using the standard bracketing technique [19]. A detailed discussion of the errors inherent in these technique is presented elsewhere [12].

3. COMPARISON WITH THEORY

Generally two methods exist for the estimation of fugacities of components in mixtures—liquid-phase activity coefficient/vapor-phase fugacity coefficient approaches and equations of state. At high pressures such as those encountered in this work, equations of state provide the simplest avenue to obtaining component fugacities. Given the equation of state as a function of volume, temperature, and composition, one must evaluate the integral

$$RT \ln \left(\frac{f_i}{x_i p} \right) = \int_0^{\rho} \left[\left(\frac{\partial p}{\partial \eta_i} \right)_{T,\rho,n_{j \neq i}} - \rho RT \right] \frac{d\rho}{\rho^2} - RT \ln Z \tag{4}$$

In this equation R is the gas constant, T is the absolute temperature, $\hat{f}_i$ is the fugacity of component i in solution, x_i is the concentration of component i, ρ is the density, and Z is the compressibility factor $p/\rho RT$.

There are two common approaches to applying this relation, one involving cubic equations of state, which incorporate mixing rules on the equation-of-state parameters for the pure fluids, and the other being the extended corresponding-states theory, which uses a "super" or reference-fluid equation of state and a conformal solution principle. In this study we have applied both of these methods, which are described below.

[2] Certain commercial equipment, instruments, or materials are identified in this paper in order to specify adequately the experimental procedure. Such identification does not imply recommendation or endorsement by the National Bureau of Standards, nor does it imply that the materials or eqipment identified are necessarily the best available for the purpose.

As an example of a cubic equation of state we have used the popular Peng–Robinson [22] modification of the Redlich–Kwong equation. This equation may be written as

$$p = \frac{RT}{v-b} - \frac{a(T_r, \omega)}{v(v+b)+b(v-b)} \tag{5}$$

where v is the molar volume and a and b are parameters for pure components which are defined by

$$a(T_r, \omega) = \Omega_a \frac{R^2 T_c^2}{p_c} \alpha(T_r, \omega)$$

$$\alpha(T_r, \omega) = 1 + m(\omega)(1 - T_r^{1/2})$$

$$m(\omega) = 0.37464 + 1.54226\omega - 0.26992\omega^2$$

and

$$b = \Omega_b \left(\frac{RT_c}{p_c}\right)$$

In these equations, Ω_a and Ω_b are universal constants, the subscript c denotes a critical-point value, T_r is the reduced temperature T/T_c, and ω is Pitzer's acentric factor defined by

$$\omega = -\log_{10}(p^0/p) - 1 \tag{6}$$

where p^0 is the vapor pressure at a reduced temperature of 0.7.

To apply this model to mixtures, one typically uses the mixing rules

$$a_{mix} = \sum_i \sum_j x_i x_j a_{ij}$$

$$b_{mix} = \sum_i \sum_j x_i x_j b_{ij} \tag{7}$$

along with the combining rules

$$a_{ij} = (a_i a_j)^{1/2} (1 - k_{ij})$$

$$b_{ij} = \frac{1}{2}(b_i + b_j) \tag{8}$$

The quantity k_{ij} is a binary interaction coefficient which is typically obtained by fitting experimental data.

Evaluating the derivative of the pressure with respect to composition and evaluating the integral given in Eq. (4), one obtains

$$\ln \frac{f_i}{x_{ip}} = \frac{B_i}{B}(z-1) - \ln(z-B) - \frac{A}{2\sqrt{2B}}\left(\frac{S_i}{A} - \frac{B_i}{B}\right) \ln\left(\frac{z+cB}{z-eB}\right)$$

where

$$\begin{aligned} A &= pa/(RT)^2 \\ B &= pb/(RT) \\ S_i &= 2\sum_j x_j a_{ij} \\ c &= 1+\sqrt{2} \qquad \text{and} \qquad e = \sqrt{2}-1 \end{aligned} \tag{9}$$

In addition to the Peng–Robinson approach, predictions were made using the simple, unmodified Redlich–Kwong equation [6], to provide a comparison with a less sophisticated model.

In the extended corresponding-states theory (EXCST) one considers the components to be conformal, e.g., species whose intermolecular potentials have the same functional form, viz.,

$$u_\alpha = f_\alpha u_o(r/h_\alpha^{1/3}) \tag{10}$$

where u denotes an intermolecular potential, r is a separation distance, and f_α and h_α are scale parameters for energy and volume, respectively. The subscript α denotes the fluid of interest and o denotes a reference substance. Assuming that the total potential energy of a collection of N molecules is pairwise additive, one finds theoretically that

$$\frac{A_j^r(V_j, T_j)}{RT_j} = \frac{A_o^r(V_o, T_o)}{RT_o} \tag{11}$$

where

$$\begin{aligned} V_o &= V_j/h_j \\ T_o &= T_j/f_j \end{aligned}$$

and

$$A^r = A(V, T) - A^*(V, T)$$

where A is the Helmholtz free energy and the asterisk denotes the ideal-gas state. All other thermodynamic properties may be obtained by differen-

tiation. Consideration of the pure-fluid critical-point criteria then leads one to the conclusions that

$$f_\alpha = (T_c^\alpha / T_c^\circ) \tag{12}$$

and

$$h_\alpha = (V_c^\alpha / V_c^\circ) \tag{13}$$

where the subscript c denotes a liquid–vapor critical-point value.

In the case of nonconformal substances, one assumes that the intermolecular potential of the fluid of interest can be made conformal to the reference substance by allowing the scale parameters f_α and h_α to be functions of temperature and density, i.e.,

$$f_\alpha = (T_c^\alpha / T_c^\circ)\, \theta(\rho, T) \tag{14}$$

$$h_\alpha = (V_c^\alpha / V_c^\circ)\, \phi_\alpha(\rho, T) \tag{15}$$

θ_α and ϕ_α are called shape factors. These factors can be related to averages of functions depending on microscopic parameters such as electrostatic moments and molecular polarizabilities.

It is interesting to note that in the case of nonconformal fluids the relations given by Eq. (11) in conjunction with Eqs. (14) and (15) are still valid, however, the relations between various thermodynamic properties become more complicated. In particular, we find the results summarized in Table I.

Table I. Dimensionless Residual Thermodynamic Properties in the Extended Corresponding-States Model with Density- and Temperature-Dependent Shape Factors[a]

Property	Relation
Helmholtz energy	$a_j^r = a_o^r$
Compressibility factor	$Z_j^r = (1 + h'_\rho)\, Z_o^r + f'_\rho u_o^r$
Internal energy	$u_j^r = (1 - f'_T)\, u_o^r - h'_T Z_o^r$
Entropy	$s_j^r = s_o^r - f'_T u_o^r - h'_T Z_o^r$
Enthalpy	$h_j^r = h_o^r + (f'_\rho - f'_T)\, u_o^r + (h_\rho - h_T)\, Z_o^r$
Gibbs energy	$g_j^r = g_o^r + h'_\rho Z_o^r + f'_\rho u_o^r$
$\ln \dfrac{f_i}{x_i \rho RT} = \dfrac{A_o^r}{RT_o} + u_o^r \dfrac{n}{f_x}\left(\dfrac{\partial f_x}{\partial n_i}\right) + Z_o^r \dfrac{n}{n_x}\left(\dfrac{\partial h_x}{\partial n_i}\right) + Z_o^r$	

[a] All energies are $x = (X - X^*)/RT$; entropy is $s = (S - S^*)/R$. All ideal-gas (*) properties are at the same density and temperature as the system. $f'_T = (\partial f/\partial T)(T/f)$, $(f'_\rho)(\rho/f)$, etc. $Z^r = pV/RT - 1$.

In order to extend the EXCST model to mixtures one must make two assumptions: (1) the dimensionless residual Helmholtz free energy $[a^r \equiv (A - A^*)/RT]$ may be equated to that of a hypothetical pure fluid; and (2) the properties of the hypothetical pure fluid can be evaluated by the corresponding-states principle just described. To perform step (1) mixing and combining rules must be adopted. For this study we have used the van der Waals one-fluid mixing rules for the f and h parameters, viz.,

$$f_x h_x = \sum_i \sum_j x_i x_j f_{ij} h_{ij}$$
$$h_x = \sum_i \sum_j x_i x_j h_{ij} \tag{16}$$

where the x denotes the hypothetical pure fluid. For combining rules we have used

$$f_{ij} = (f_i f_j)^{1/2} (1 - k_{ij})$$
$$h_{ij} = \frac{1}{8} (h_i^{1/3} + h_j^{1/3})^3 (1 - l_{ij}) \tag{17}$$

The reference-fluid equation of state used in this work was the 32-term BWR (Benedict, Webb, Rubin)-type equation [23] for propane. The functional form of the equation is given in Table II. Typically, the propane

Table II. Functional Form of 32-Term BWR[a]

$$p = \sum_{n=1}^{9} \partial n(T)\, \rho^n + e^{-\gamma\rho^2} \sum_{n=10}^{15} \partial n(T)\, \rho^{2n-17}$$

$a_1 = RT$
$a_2 = b_1 T + b_2 T^{1/2} + b_3 + b_4/T + b_5/T^2$
$a_3 = b_6 T + b_7 + b_8/T + b_9/T^2$
$a_4 = b_{10} T + b_{11} + b_{12}/T$
$a_5 = b_{13}$
$a_6 = b_{14}/T + b_{15}/T^2$
$a_7 = b_{16}/T$
$a_9 = b_{19}/T^2$
$a_{10} = b_{20}/T^2 + b_{21}/T^3$
$a_{11} = b_{22}/T^2 + b_{23}/T^4$
$a_{12} = b_{24}/T^2 + b_{24}/T^3$
$a_{13} = b_{26}/T^2 + b_{27}/T^4$
$a_{14} = b_{28}/T^2 + b_{29}/T^3$
$a_{16} = b_{30}/T^2 + b_{32}/T^4$

[a] R is the gas constant and T is the absolute temperature in K.

equation reproduces the experimental densities to within 0.3% and the pressures to within 2.5%. As usual, the greatest density errors are in the critical region, while the largest pressure errors are in the low-temperature liquid region.

Examination of the equations in Table I shows that it is not possible to calculate shape factors unambiguously from experimental thermodynamic data. Since we need to find two shape factors, θ_i and ϕ_i (or equivalently f_i and h_i), we need two equations to solve. If one chooses the equations for the Helmholtz energy and the compressibility factor,

$$\begin{aligned} a_j^r(\rho_j, T_j) &= a_o(\rho_o, T_o) \\ Z_j^r &= (1+h_\rho)\, Z_o^r + u_o^r f_\rho \end{aligned} \tag{18}$$

The derivatives of f and h enter the calculation, i.e., the thermodynamic relationships provide an undetermined system of equations. In order to perform the calculations of f_j and h_j we must therefore (arbitrarily) choose a particular set.

The most convenient set computationally is that obtained when we require $Z_o^r = Z_j^r$, i.e., the set of solutions for the case where the density derivatives of f and h satisfy the relation

$$Z_o^r h_\rho = -u_o^r f_\rho \tag{19}$$

Thus, to obtain exact shape factors we solve

$$\begin{aligned} a_j^r(\rho_j, T_j) &= a_o^r(\rho_o, T_o) \\ Z_j^r(\rho_j, T_j) &= Z_o^r(\rho_o, T_o) \end{aligned} \tag{20}$$

for ρ_o and T_o given ρ_j, T_j and accurate equations of state for the pVT behavior of fluids j and o. This solution may be easily accomplished numerically using a two-dimensional Newton–Raphson iteration.

Shape factors have been evaluated by this procedure for 12 fluids: methane, ethane, propane, *i*-butane, *n*-butane, carbon dioxide, nitrogen, oxygen, argon, ethylene, hydrogen, and nitrogen trifluoride. In addition, data for systems with larger acentric factors than those listed above were required. They were generated using saturated liquid density and vapor pressure data and solving the equation

$$p_o^s = p_j^s(T_j)\, \rho_o^s(T_j/f_j)/f_j \rho_j^s(T_j) \tag{21}$$

The resulting functional forms for the propane shape factors are

$$\begin{aligned} \theta &= 1 + (\omega - \omega_o)[a - b \ln T_r] \\ \phi &= \{1 - (\omega - \omega_o)[c - d \ln T_r]\} \frac{Z_c^o}{Z_c} \end{aligned} \tag{22}$$

Table III. Fugacity Coefficients for the Hydrogen + Propane System at 80°C (353 K) and a Mixture Pressure of 3.45 MPa

Hydrogen mole fraction, x_{H_2}	Fugacity coefficient, $\phi^m_{H_2}$
0.8481	1.04
0.8215	1.033
0.7298	1.028
0.6588	1.036
0.5935	1.058
0.5261	1.08
0.4452	1.106
0.344	1.17
0.3088	1.23
0.2801	1.283

The fact that the resulting shape factors are independent of density is advantageous from a computational point of view in that the density derivatives of f and h in Table I are zero, thereby removing the need for iterative density calculations in evaluating Eqs. (16).

4. RESULTS AND DISCUSSION

Component fugacity coefficients of hydrogen in propane, $\phi^m_{H_2}$, at 80°C (353 K) and 130°C (403 K) are presented in Tables III and IV. In both cases the total mixture pressure was 3.45 MPa. Plots of $\phi^m_{H_2}$ versus the mole fraction of hydrogen are presented in Figs. 2 and 3. The error bars in the figures indicate the uncertainty of a $\phi^m_{H_2}$–x_{H_2} pair for an equimolar mixture.

Table IV. Fugacity Coefficients for the Hydrogen + Propane System at 130°C (403 K) and a Mixture Pressure of 3.45 MPa

Hydrogen mole fraction, x_{H_2}	Fugacity coefficient, $\phi^m_{H_2}$
0.8354	1.038
0.7827	1.047
0.618	1.077
0.5449	1.096
0.4718	1.116
0.2649	1.22

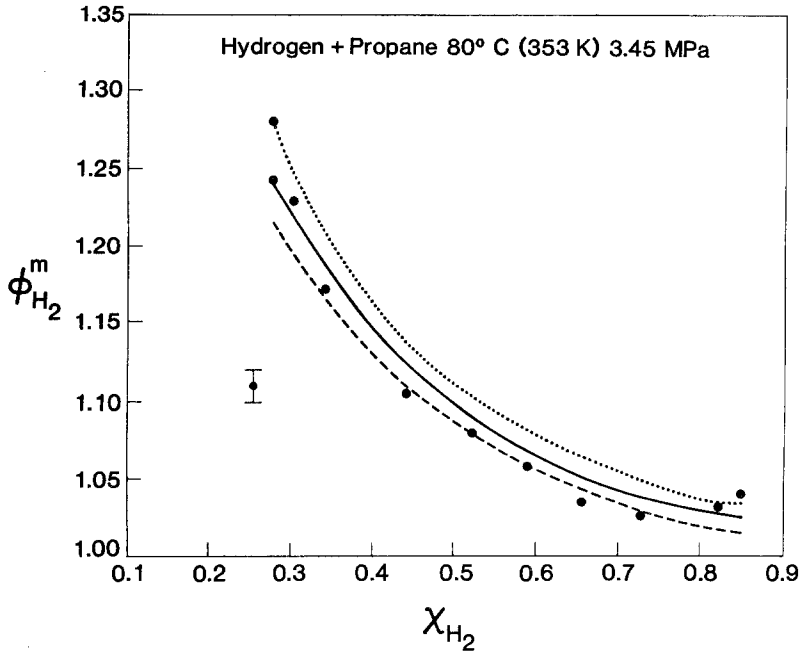

Fig. 2. Plot of $\phi^m_{H_2}$ vs x_{H_2} for hydrogen + propane at 80°C (353 K) and 3.45 MPa. ●, Experimental data; solid line, Redlich–Kwong; dashed line, Peng–Robinson; dotted line, EXCST. The error bar shown in the figure represents a typical uncertainty, and is not a data point.

A detailed error analysis describing how the magnitude of the uncertainty was arrived at has been provided previously [12].

Component fugacity coefficients of hydrogen in methane at 80°C (353 K) and 3.45 MPa of total pressure are presented in Table V. A plot of $\phi^m_{H_2}$ versus x_{H_2} is presented in Fig. 4.

Before examining the agreement of the experimental results with those predicted using the equations of state, some general qualitative observations can be made. In the plots for both the propane and the methane mixtures, the change of $\phi^m_{H_2}$ is most pronounced at lower values of the hydrogen mole fraction. This behavior is consistent for a low molecular weight gas (at a relatively high reduced temperature) in a binary mixture with a heavier gas. The same general trend was observed in other studies on hydrogen + propane [24] and hydrogen + carbon dioxide [25] binary mixtures.

The behavior of the hydrogen + propane isotherms as a function of temperature is also of interest. At the higher temperature, $\phi^m_{H_2}$ shows a more gradual increase in slope (as x_{H_2} decreases) than at the lower temperature.

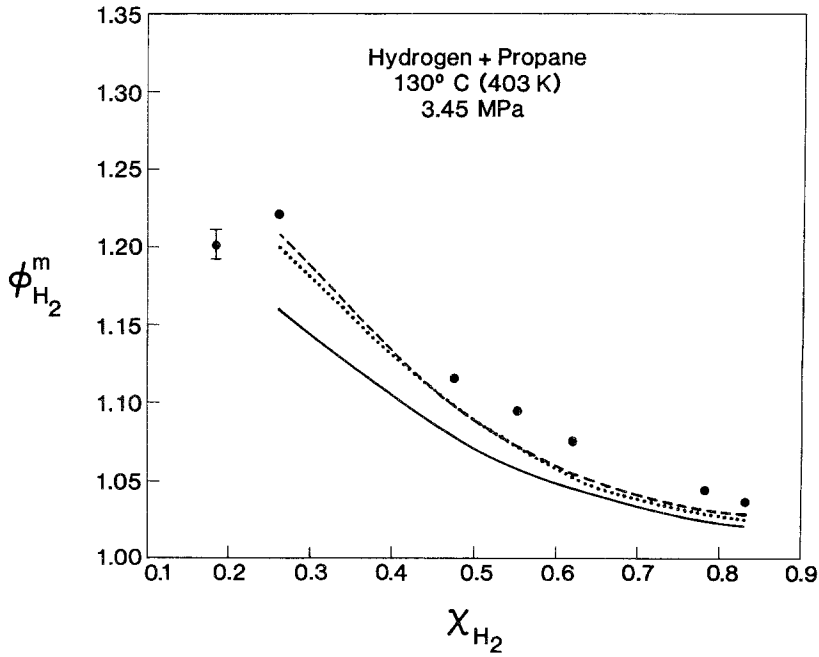

Fig. 3. Plot of $\phi^m_{H_2}$ vs x_{H_2} for hydrogen + propane at 130°C (403 K) and 3.45 MPa. ●, Experimental data; solid line, Redlich–Kwong; dashed line, Peng–Robinson; dotted line, EXCST. The error bar shown in the figure represents a typical uncertainty, and is not a data point.

Table V. Fugacity Coefficients for the Hydrogen + Methane System at 80°C (353 K) and a Mixture Pressure of 3.45 MPa

Hydrogen mole fraction, x_{H_2}	Fugacity coefficient, $\phi^m_{H_2}$
0.8494	1.121
0.7901	1.115
0.7637	1.097
0.6515	1.115
0.5355	1.125
0.4594	1.134
0.3065	1.166
0.2155	1.223

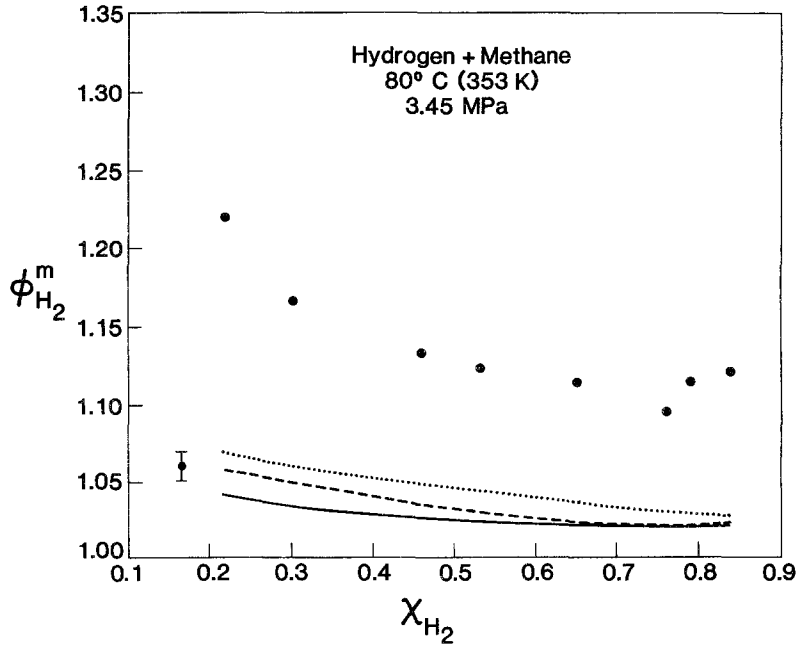

Fig. 4. Plot of $\phi^m_{H_2}$ vs x_{H_2} for hydrogen + methane at 80°C (353 K) and 3.45 MPa. ●, Experimental data; solid line, Redlich–Kwong; dashed line, Peng–Robinson; dotted line, EXCST. The error bar shown in the figure represents a typical uncertainty, and is not a data point.

In addition, the total change in $\phi^m_{H_2}$ over a given range of x_H is much less at the higher temperature than at the lower temperature. This observation is consistent with the expectation that $\phi^m_{H_2}$ should be closer to unity at higher temperatures, for a given gas composition. Comparing the results of the methane and propane binaries at 80°C, one notices a much greater total change in $\phi^m_{H_2}$ for the propane system (23% over the mole-fraction range) than for the methane system (13% over the mole-fraction range). This is expected because of the higher reduced temperature of methane. Measurements on the hydrogen + methane system were not performed above 80°C since the change in $\phi^m_{H_2}$ would be quite small.

In Figs. 2 through 4, the data measured in this study (represented by the filled circles) are compared with the predictive methods described in the previous section. The values calculated using the Redlich–Kwong equation are represented by the solid line, the values calculated using the Peng–Robinson equation are represented by the dashed line, and the values calculated using the EXCST approach are represented by the dotted line.

For the 80°C (353 K) isotherm of the hydrogen + propane system, all of the equations of state give acceptable predictions for $\phi^m_{H_2}$. The Redlich–

Kwong equation, despite its inherent simplicity, gives excellent predictions of the experimental values, with deviations of between 1.0 and 0.2%. The Peng–Robinson equation also gives good predictions, but with slightly more scatter. In this approach, the acentric factor for hydrogen was assigned a value of −0.22, which is experimentally indicated [26]. The EXCST approach shows the most significant deviations from the experimental data, although the predictions are still acceptable. Here, the acentric factor was assigned a value of −0.22 [26], and the binary interaction coefficients as determined experimentally (from binary vapor–liquid equilibrium measurements) were applied [27]. It should be noted that the predicted values of $\phi_{H_2}^m$ are not a sensitive function of either the acentric factor or the interaction coefficients. The calculated values are usually within 1% as long as physically reasonable values of these parameters are employed.

For the 130°C (403 K) isotherm, larger deviations are observed between the experimental and the predicted values, however, the predictions are still acceptable. The slightly poorer agreement is somewhat surprising, since at the higher temperature, both the experimental apparatus and the equations of state are expected to perform better than at lower temperatures. For this isotherm, the Redlich–Kwong equation gives the worst predictions, with deviations of between 4.0 and 1.0%. The extended corresponding-states approach gives the best predictions (with deviations of between 2.0 and 0.2%). The predictions of the Peng–Robinson equation are slightly poorer than those of the EXCST approach. For this isotherm, adjustment of the accentric factor and (in the case of EXCST) the interaction coefficients was found to have a negligible effect.

Figure 4 compares the predictions for the hydrogen + methane 80°C (353 K) isotherm. In this case the predictions are generally not acceptable, with deviations reaching as high as 15 to 20%. This is especially true in the range of low hydrogen mole fractions. The high deviations in this range are at least partly due to the lower precision of the hydrogen quantitation at low mole fractions [24, 25]. We also note in passing that the hydrocarbon component in this case is highly supercritical ($T_r \approx 2$ for methane) compared to the propane case, where $T_r \cong 1$. This might indicate that the models investigated here have structural failures at higher reduced temperatures. Studies are currently under way to attempt improved representation of this system.

5. CONCLUSIONS

Fugacity coefficients for the hydrogen + propane binary (along two isotherms) and the hydrogen + methane binary (along one isotherm) were

measured, at a mixture pressure of 3.45 MPa. The experimental data were used to evaluate the predictive capability of three equations of state. Acceptable predictions were obtained for both isotherms of the hydrogen + propane system. The predictions for the hydrogen + methane system were unacceptably low for each equation of state. Possible modifications to the equations of state are now being considered in order to obtain better predictions for this system.

ACKNOWLEDGMENTS

The authors would like to acknowledge the assistance of Lysette Hunt in performing some of the calculations. The financial support of the Gas Research Institute is gratefully acknowledged.

REFERENCES

1. G. N. Lewis, *Proc. Am. Acad.* **37**:49 (1901).
2. G. N. Lewis, *Z. Phys. Chem.* **38**:205 (1901).
3. G. N. Lewis and M. Randall, *Thermodynamics* (McGraw–Hill, New York, 1961).
4. S. I. Sandler, *Chemical and Engineering Thermodynamics* (John Wiley & Sons, New York, 1977).
5. B. G. Kyle, *Chemical and Process Thermodynamics* (Prentice Hall, Englewood Cliffs, N.J., 1984).
6. J. M. Prausnitz, *Molecular Thermodynamics of Fluid Phase Equilibria* (Prentice Hall, Englewood Cliffs, N.J., 1969).
7. K. Denbigh, *The Principles of Chemical Equilibrium* (Cambridge University Press, New York, 1971).
8. J. M. Prausnitz, *AIChE J.* **5**:3 (1969).
9. H. Y. Cheh, *Proceedings of the 6th Symposium on Thermophysical Properties*, P. E. Liley, ed. (Am. Soc. Mech. Eng., New York, 1973), p. 256.
10. D. P. Smith, *Hydrogen in Metals* (University of Chicago Press, Chicago, 1948).
11. E. M. Wise, *Palladium* (Academic Press, New York, 1968).
12. T. J. Bruno, *J. Res. Natl. Bur. Std.* **90**(2):127 (1985).
13. T. J. Bruno, *J. Chromatogr. Sci.* **23**(7):325 (1985).
14. T. J. Bruno and G. L. Hume, *J. Res. Natl. Bur. Std.* **90**(3):225 (1985).
15. *ASME Boiler and Pressure Vessel Code, Sect. VIII: Unfired Pressure Vessels* (American Society of Mechanical Engineers, New York, 1965).
16. R. L. Powell, W. J. Hall, C. H. Hyink, L. L. Sparks, G. W. Burns, M. G. Scroger, and H. H. Plumb, *Thermocouple Reference Tables Based on the IPTS-68*, National Bureau of Standards, Monograph 125 (1975).
17. T. J. Bruno, D. E. Martire, M. W. P. Harbison, A. Nikolić, and C. F. Hammer, *J. Phys. Chem.* **87**:2425 (1983).
18. E. Heftmann, *Chromatography: A Laboratory Handbook of Chromatographic and Electrophoretic Methods*, 3rd ed. (Van Nostrand Reinhold, New York, 1975).
19. H. M. McNair and E. J. Bonnelli, *Basic Gas Chromatography* (Varian Aerograph, 1969).
20. C. J. Cowper and A. J. DeRose, *The Analysis of Gases by Chromatography* (Pergamon Press, Oxford, 1983).

21. P. G. Jeffery and P. J. Kiping, *Gas Analysis by Gas Chromatography* (Pergamon Press, Oxford, 1972).
22. D.-Y. Peng and D. B. Robinson, *Ind. Eng. Chem. Fund.* **15**:59 (1976).
23. R. T. Jacobsen and R. J. Stewart, *J. Phys. Chem. Ref. Data* **2**:757 (1973).
24. F. Antezana and H. Y. Cheh, *Ind. Eng. Chem. Fund.* **14**:224 (1975).
25. T. J. Bruno and G. L. Hume, *Int. J. Thermophys.* **7**:1053 (1986).
26. R. C. Reid, J. M. Prausnitz, and T. K. Sherwood, *The Properties of Gases and Liquids* (McGraw–Hill, New York, 1976), p. 630.
27. R. A. Mentzer, R. A. Greenkorn, and K.-C. Chao, *Ind. Eng. Chem. Process Des. Dev.* **20**:240 (1981).